

Novel β -diketonate complexes of Eu^{3+} bearing pyrazole moiety for bright photo- and electroluminescence



V.M. Korshunov^{a,c,*}, S.A. Ambrozevich^{a,b,c}, I.V. Taydakov^{a,b,d}, A.A. Vashchenko^{a,b},
D.O. Goriachiy^a, A.S. Selyukov^{a,b}, A.O. Dmitrienko^d

^a P. N. Lebedev Physical Institute of the Russian Academy of Sciences, Leninskiy Prospect 53, 119991, Moscow, Russia

^b Moscow Institute of Physics and Technology (State University), Institutskiy Per. 9 Institutskiy per., Dolgoprudny, Moscow Region, 141701, Russian Federation

^c Bauman Moscow State Technical University, 2-ya Baumanskaya Str. 5/1, 105005, Moscow, Russia

^d A. N. Nesmeyanov Institute of Organoelement Compounds of the Russian Academy of Sciences, Vavilova St. 28, 119991, GSP-1 V-334, Moscow, Russia

ARTICLE INFO

Keywords:

Eu^{3+}
Coordination compounds
 β -diketonates
OLED
Electroluminescence
Fluorination
Sensitization efficiency

ABSTRACT

Four novel 1,3-diketonate Eu^{3+} complexes bearing pyrazole moieties as main ligands and a 4,7-Diphenyl-1,10-phenanthroline (bathophenanthroline) ancillary ligand were synthesized. The number of fluorine atoms in the main ligand was varied from 3 to 13. From spectroscopic studies of the synthesized complexes we conclude that increasing the degree of fluorination results in a significant rise in the quantum yield and sensitization efficiency. With further extension of the fluorinated chain length, saturation of these characteristics was observed. The maximum obtained values of the quantum yield and sensitization efficiency were 56% and 99%, respectively. In order to reveal the potential of the complexes for OLED applications, electroluminescent devices based on these compounds were fabricated and their performance was studied. It was found that the quantum efficiencies of the OLEDs and the sensitization efficiencies exhibit similar behaviour depending on the degree of fluorination of the ligands in the complexes.

1. Introduction

The search for efficient and stable luminescent materials to be used in displays and lighting is an extremely important and challenging task. Lanthanide complexes with organic ligands [1,2] as well as other metalorganic compounds [3,4] appear to be promising in this respect. The enduring interest of the scientific community is drawn by a number of essential effects (particularly, the “antenna” effect) specific to these compounds, as well as by their highly efficient luminescence. In these compounds the sensitization efficiency of the ion emission can be as high as 100% [5]. Moreover, attractive optical properties of the lanthanide complexes such as narrow emission bands and high quantum yields are combined with relative simplicity of their synthesis.

The physics behind the luminescence of lanthanide complexes resides in the violation of the selection rules for the transitions between $4f$ levels of the ion. The luminescence efficiency is governed by the processes of energy transfer from the ligand environment to the ion, as well as by the excitation quenching [6]. The latter process can lead to decreased quantum yields due to vibrational relaxation via OH, CH, and NH oscillations in the complexes [6,7].

As demonstrated for Eu^{3+} and Tb^{3+} ions, it is possible to partially suppress multiphonon quenching in the ligands by introduction of low-frequency oscillators, e.g. by replacing the CH bonds with CF ones [8,9]. It is also important to remove the solvent molecules from the inner coordination sphere of the ion, since they can cause additional quenching. This is achieved by the employment of ancillary ligands [10].

The development of the synthesis protocols and design procedures promoting suppression of quenching and enhancement of the energy transfer from the ligand environment to the ion would facilitate successful implementation of the lanthanide complexes with β -diketonate ligand environment in the OLED technology, providing the devices with superior operational characteristics [11–14]. For example, in Ref. [15] we obtained the turn-on voltage as low as 3.5 V for the OLED based on a Eu^{3+} complex.

In the present paper we have investigated four Eu^{3+} complexes with β -diketonate main ligands and a 4,7-Diphenyl-1,10-phenanthroline (bathophenanthroline) ancillary ligand. The effect of increasing the degree of fluorination on photo- and electroluminescent properties of the synthesized compounds was studied.

* Corresponding author. P. N. Lebedev Physical Institute of the Russian Academy of Sciences, Leninskiy Prospect 53, 119991, Moscow, Russia.

E-mail addresses: vladkorshunov@sci.lebedev.ru (V.M. Korshunov), s.ambrozevich@mail.ru (S.A. Ambrozevich), taidakov@mail.ru (I.V. Taydakov), andrewx@mail.ru (A.A. Vashchenko), gor-dog1993@mail.ru (D.O. Goriachiy), selyukov@sci.lebedev.ru (A.S. Selyukov), dmitrienka@gmail.com (A.O. Dmitrienko).

<https://doi.org/10.1016/j.dyepig.2018.12.006>

Received 9 October 2018; Received in revised form 8 November 2018; Accepted 5 December 2018

Available online 10 December 2018

0143-7208/ © 2018 Elsevier Ltd. All rights reserved.

2. Experimental

2.1. Materials and methods

The ligands were obtained by condensation of the corresponding pyrazolic ketones and ethyl esters in the presence of NaH as a base, according to the previously published procedure [16]. Europium (III) oxide (99.99%) and all other reagents and solvents were purchased from Aldrich and used without additional purification.

Elemental analysis was performed on an Elementar Vario MicroCube CHNO(S) analyzer. The metal content was determined by complexometric titration with a Trilon B solution in the presence of Xylenol Orange as an indicator. Before the analysis, the complexes were decomposed by heating with concentrated HNO₃. Nuclear magnetic resonance (NMR) spectra were recorded for CDCl₃ solutions of the complexes at 298 K on a Bruker AC-300 instrument operated at 300.13 and 282.40 MHz for ¹H and ¹⁹F nuclei, respectively. TMS ($\delta = 0.00$ ppm) was used as a standard for ¹H measurements and CFCl₃ ($\delta = 0.00$ ppm) was taken as an external standard for ¹⁹F measurements. Infrared spectra were measured in KBr pellets on a Bruker Tensor 27 FTIR (Fourier-transform infrared spectroscopy) instrument. Thermogravimetric analysis and differential scanning calorimetry (TGA/DSC) was performed on a TA Instruments SDT Q600 analyzer in air (100 mL/min).

For X-ray powder diffraction data collection, the samples were placed between two polyimide films and mounted into a Bruker AXS D8 Advance Vario X-ray powder diffractometer equipped with a primary monochromator (Cu – K α_1 , $\lambda = 1.54056 \text{ \AA}$) and a LynxEye PSD. The data were collected in the transmission mode at ambient temperature for $2\theta = 2\text{--}90^\circ$ with a step size of 0.01° . The diffraction patterns were indexed using the SVD (singular value decomposition) index algorithm [17] as implemented in the Bruker TOPAS 5.0 software [18], the space group was determined using the analysis of systematic absences, and the cell parameters were refined using the Pawley method.

Optical absorption spectra were recorded at ambient temperature with the use of a Specord M40 spectrophotometer operating within 200–800 nm. The experiments were carried out for the complexes and corresponding neat ligand bathophenanthroline in the solutions poured into 1-cm-pathlength quartz optical cells. The samples were dissolved in acetonitrile (HPLC-grade super gradient, Panreac, Spain) with concentrations of about 5×10^{-6} mol/l.

Photoluminescence (PL) spectra were obtained at ambient temperature with an Ocean Optics Maya 2000 Pro CCD spectrometer sensitive within 200–1100 nm and a Perkin-Elmer LS-45 spectrofluorimeter equipped with a Hamamatsu R928 photomultiplier sensitive within 200–900 nm. In the photoluminescence experiments involving the CCD spectrometer, a 365 nm CW laser was employed as the excitation source. To resolve the fine structure of the lanthanide ion luminescence (if needed), additional PL measurements were carried out at 77 K. The excitation spectra were obtained using an experimental setup based on SDL-1 and MDR-23 monochromators installed in the registration and excitation channels of the system, respectively. A 2 kW xenon lamp was used for excitation. The detector was a Hamamatsu H8259-01 photomultiplier. Luminescence decays were measured using the SDL-1 monochromator and a Lotis TII LS-2134 Nd:YAG pulsed laser emitting at 355 nm with 5 ns pulse duration, 12 Hz repetition rate, and 40 mJ average pulse energy. PL spectra and PL decays were measured for polycrystalline samples sandwiched between two quartz slides. Excitation spectra were obtained for polycrystalline samples and solutions of the complexes in acetonitrile.

To measure the absolute luminescence quantum yield (QY) we used a Horiba Jobin-Yvon Fluorolog FL3-22 spectrofluorimeter equipped with a G8 Spectralon[®]-covered sphere (GMP SA, Switzerland) and a

Hamamatsu R928 photomultiplier. A diffusing screen was mounted inside the sphere to avoid direct irradiation of the detector. The setup provided a means to investigate powder samples emitting within 450–800 nm. The measurements were carried out at ambient temperature. The samples in quartz cells were placed near the centre of the sphere. An emission-standard 45 W quartz tungsten-halogen lamp (Oriel) was employed to measure the instrument response function.

2.2. Synthesis

Stock 0.5 M solution of EuCl₃ was prepared by the treatment of Eu₂O₃ (4.400 g, 12.50 mmol) by minimum amount of concentrated HCl in a quartz crucible. The resulting solution was evaporated to dryness at 90 °C and the residue was dissolved in a minimum amount of distilled water. After that, the solution was transferred quantitatively to a volumetric flask and the volume was adjusted to 50 mL. This solution was then kept in a polypropylene flask. To a stirred warm (40 °C) solution of the ligand (3 mmol) and (1 mmol) bathophenanthroline (0.33 g) in 30 mL of ethanol, 2 mL of an 0.5 M aqueous solution of EuCl₃ (1 mmol) were added dropwise, followed by careful addition of 3 mL (3 mmol) of an 1.0 M NaOH solution in water until the pH of the mixture reached 6–7. The mixture was heated at 50 °C during 4 h in a closed flask and cooled. Further operations depended upon the properties of the reaction products.

2.2.1. Complex A: (1-(1,3-Dimethyl-1H-pyrazol-4-yl)-4,4,4-trifluorobutane-1,3-dionato)(4,7-diphenyl-1,10-phenanthroline) europium (III)

The reaction mixture was evaporated to dryness and extracted by hot 2-propanol (30 mL). The resulting solution was filtered, concentrated to a small volume (2 mL), and left for 4 weeks in a closed container. The crystals were separated, washed with a small amount of cold MeOH, and dried to constant weight at 10^{-2} Torr and 40 °C.

The yield was 0.45 g (38%) of a light yellow powder. Anal. Calcd. for C₅₁H₄₀EuF₃N₈O₆ (1183.86): C, 51.74; H, 3.41; N, 9.47, Eu, 12.84%. Found: C, 51.99; H, 3.63; N, 9.81, Eu 12.93%. FTIR (KBr, cm⁻¹): 1615, 1597, 1571 (ν_s C=O); 1331 (ν_s C–N); 1306, 1181 (ν_s CF). ¹H NMR (300 MHz, CDCl₃): δ 9.74 (br. s, 2H), 8.91 (br. s, 4H), 8.57 (m, 4H), 8.26 (m, 5H), 8.03 (br. s, 4H), 6.09 (br. s, 3H, CH=CO), 4.94 (br. s, 9H, N–CH₃), 3.83 (br. s, 9H, CH₃). ¹⁹F NMR (282.5 MHz, CDCl₃): –81.31 (s, 9H, CF₃).

2.2.2. Complex B: (4,4,5,5-Tetrafluoro-1-(1-methyl-1H-pyrazol-4-yl)pentane-1,3-dionato)(4,7-diphenyl-1,10-phenanthroline) europium (III)

The reaction mixture was evaporated to dryness and extracted by hot CH₂Cl₂ (20 mL). The solution was evaporated to dryness and the residue was dissolved in 5 mL of hot 2-propanol. The solution was kept at room temperature overnight. Spontaneous crystallization of the complex occurred upon standing. The precipitate was separated, washed successively with a small amount of cold 2-propanol and hexane, and finally dried to constant weight at 10^{-2} Torr and 40 °C.

The yield was 0.76 g (61%) of a tan powder. Anal. Calcd. for C₅₁H₃₇EuF₁₂N₈O₆ (1237.83): C, 49.49; H, 3.01; N, 9.05, Eu 12.2%. Found: C, 49.67; H, 2.86; N, 10.14, Eu 12.41%. FTIR (KBr, cm⁻¹): 1637, 1561 (ν_s C=O); 1353 (ν_s C–N); 1255, 1159 (ν_s CF). ¹H NMR (300 MHz, CDCl₃): δ 9.46 (br. s, 2H), 9.15 (br. s, 2H), 8.77 (m, 4H), 8.19 (br. s, 7H), 7.97 (m, 4H), 7.47 (br. s, 3H), 7.13 (br. s, 3H, CH=CO), 5.09 (t, 1H, $J = 53.6$ Hz, CHF₂) 4.01 (br. s, 9H, N–CH₃). ¹⁹F NMR (282.5 MHz, CDCl₃): –132.23 (br. s, 6F, CF₂), –140.95 (d, 6F, $J = 47.3$ Hz, CHF₂).

2.2.3. Complex C: (4,4,5,5,6,6,6-Heptafluoro-1-(1-methyl-1H-pyrazol-4-yl)hexane-1,3-dionato)(4,7-diphenyl-1,10-phenanthroline) europium (III)

The reaction mixture was evaporated to dryness and extracted by hot CH₂Cl₂ (20 mL). The resulting solution was filtered, concentrated to

a small volume (3 mL), and hexane was carefully added in small portions with stirring. The precipitated oil solidified upon standing. The solid complex was separated, washed with hexane, and dried to constant weight at 10^{-2} Torr and 40°C .

The yield was 0.81 g (56%) of a light yellow powder. Anal. Calcd. for $\text{C}_{54}\text{H}_{34}\text{EuF}_{21}\text{N}_8\text{O}_6$ (1441.83): C, 44.98; H, 2.38; N, 7.77, Eu 10.54%. Found: C, 45.11; H, 2.28; N, 7.96, Eu 10.68%. FTIR (KBr, cm^{-1}): 1623, 1601, 1591 ($\frac{1}{2}$ C=O); 1339 ($\frac{1}{2}$ C–N); 1277, 1211 ($\frac{1}{2}$ CF). ^1H NMR (300 MHz, CDCl_3): δ 10.79 (br. s, 2H), 9.46 (br. s, 2H), 8.81 (s, 4H), 8.48 (br. s, 2H), 8.22 (br. s, 4H), 7.99 (br. s, 4H), 7.75 (br. s, 4H), 7.28 (br. s, 3H, CH=CO), 4.10 (br. s, 9H, N–CH₃). ^{19}F NMR (282.5 MHz, CDCl_3): –81.21 (br. s, 9F, CF₃), –125.80 (br. s, 6F, CF₂), –128.41 (br. s, 6F, CF₂).

2.2.4. Complex D: (4,4,5,5,6,6,7,7,8,8,9,9,9-Tridecafluoro-1-(1-methyl-1H-pyrazol-4-yl)nonane-1,3-dionato)(4,7-diphenyl-1,10-phenanthroline) europium (III)

The reaction mixture was evaporated to dryness and the crystalline solid was boiled in heptane (20 mL). Absolute EtOH was added dropwise to this suspension until all tarry impurities were dissolved. The suspension was cooled to room temperature, the precipitate was separated and successively washed with hexane, small amount of MeOH and water on a filter. The solid material was then dried to constant weight at 10^{-2} Torr and 40°C .

The yield was 1.47 g (78%) of a fine white powder. Anal. Calcd. for $\text{C}_{63}\text{H}_{34}\text{EuF}_{39}\text{N}_8\text{O}_6$ (1891.90): C, 40.00; H, 1.81; N, 5.91, Eu 8.03%. Found: C, 40.51; H, 1.97; N, 6.24, Eu 8.37%. FTIR (KBr, cm^{-1}): 1621, 1553 ($\frac{1}{2}$ C=O); 1366 ($\frac{1}{2}$ C–N); 1209, 1154 ($\frac{1}{2}$ CF). ^1H NMR (300 MHz, CDCl_3): δ 9.30 (br. s, 2H), 8.81 (br. s, 2H), 8.48 (s, 4H), 8.22 (br. s, 2H), 8.22 (br. s, 4H), 7.99 (br. s, 4H), 7.71 (br. s, 4H), 6.68 (br. s, 3H, CH=CO), 4.01 (br. s, 9H, NCH₃). ^{19}F NMR (282.5 MHz, CDCl_3): –81.51 (br. s, 9F, CF₃), –121.38 (br. s, 6F, CF₂), –122.12 (br. s, 6F, CF₂), –123.21 (br. s, 6F, CF₂), –123.52 (br. s, 6F, CF₂), –126.88 (br. s, 6F, CF₂).

Structural formulae of the synthesized complexes are given in Fig. 1.

2.3. Device fabrication and characterization

Poly(3,4-ethylenedioxythiophene):poly(styrenesulfonic acid) (PEDOT:PSS) hole injection material, 2,2'-Dimethyl-N,N'-di-[(1-naphthyl)-N,N'-diphenyl]-1,1'-biphenyl-4,4'-diamine (α -NPD) hole transport material, 4,4'-Bis(N-carbazolyl)-1,1'-biphenyl (CBP) host layer material, 1,3,5-tris[N-(phenyl)benzimidazole]-benzene (TPBi) electron transport material as well as LiF and Al cathode materials were purchased from Luminescence Technology Corp. and used without further purification.

ITO-coated glass substrates were washed in an alcohol solution of KOH followed by the ultrasonic treatment in bidistilled water for 20 min. The substrates were dried in a flow of nitrogen. After that a 50-nm-thick PEDOT:PSS layer was deposited by spin-coating with further annealing in air at 120°C for 20 min. The substrates were then

transferred to an argon-filled glovebox equipped with a Leybold-Heraeus Univex 300 vacuum deposition chamber. The layers of α -NPD, TPBi, LiF, and Al were deposited by thermal evaporation in vacuum (residual pressure below 10^{-3} Pa). OLED active layers were deposited by thermal coevaporation of CBP and the corresponding Eu complexes (10:1 wt ratio). The deposition thickness was controlled by a Leybold Inficon IC-6000 deposition controller. The controller was calibrated by deposition of reference films with the subsequent measurement of their thicknesses with the use of an NT-MDT Integra atomic force microscope.

The luminance of the OLED samples was measured by a TKA-PKM luminance meter produced by TKA Scientific Instruments. Current-voltage characteristics were obtained using an automated setup involving a Keitley 6485 picoammeter, Agilent 34401A voltmeter, and a Motech 2019 power supply. OLED optical power was determined using a Coherent FieldMaxII Laser Power Meter with a calibrated photodiode head. Electroluminescence (EL) spectra were obtained with an Ocean Optics Maya 2000 Pro CCD spectrometer.

3. Results and discussion

3.1. Thermogravimetric analysis

The thermograms of the complexes are similar in shape and show one main step of weight loss, which is consistent with decomposition and combustion of the organic ligands (see Fig. 9 in the Supplementary materials). Thermal stability of the complexes strongly depends upon the ligand structures. Complex A starts to decompose in air at temperatures of about 130°C , while complexes C and D are rather stable up to 300°C . Complex B is more stable than complex A and its degradation starts at 248°C . The first step of decomposition of all complexes is associated with evaporation of the ligands. Small endothermic effects observed for complexes B, C, and D (at 120, 182, and 162°C , respectively) correspond to melting. It is worth mentioning that a small endothermic peak at 125°C seen for complex D can be assigned to formation of a mesophase; this phenomenon is known for the complexes, bearing long perfluorinated chains [19]. The main decomposition step starts between 460 and 517°C depending on the nature of the complex. Decomposition is accomplished with a strong exothermic effect associated with vigorous oxidation of the organic matter. The weight of the residue after decomposition of all four complexes corresponds to formation of EuF_3 rather than Eu_2O_3 . The small exothermic effect observed near 730°C can be attributed to recrystallization of EuF_3 . Thermal stability of the complexes increases with increasing the degree of fluorination of the alkyl chain and the complexes with the substituents of a moderate length (C, D) are preferable for deposition of the OLED active layers by thermal evaporation.

3.2. Analysis of IR spectra

IR spectra of the complexes are similar, exhibiting C=O and C=C stretching vibrations at 1659 and 1517 cm^{-1} , respectively, which are

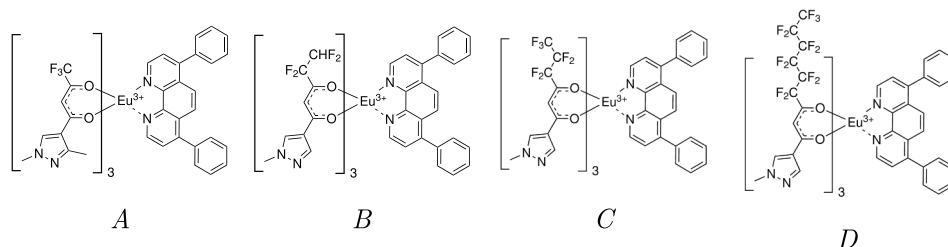


Fig. 1. Structural formulae of investigated complexes A–D.

Table 1
Unit cell parameters for complexes A–D.

Crystal System	complex A	complex B	complex C	complex D
	Monoclinic	Monoclinic	Monoclinic	Triclinic
Space group	$P2_1c$	Cc	$P2_1c$	$P-1$
a, Å	11.8710 (6)	24.835 (7)	14.7222 (9)	14.596 (19)
b, Å	42.077 (3)	20.1756 (18)	39.351 (3)	16.51 (2)
c, Å	10.4848 (6)	11.1576 (17)	11.2680 (4)	21.45 (2)
α , °	90.	90.	90.	98.20 (8)
β , °	89.632 (5)	107.83 (4)	63.922 (3)	117.32 (8)
γ , °	90.	90.	90.	99.33 (9)
Volume, Å ³	5236 (6)	5322 (2)	5863.3 (6)	4392 (11)

typical of lanthanide chelate complexes containing fluorinated β -diketone ligands. The bands for the C=C and C=N ring vibrations appear in the region of 1650–1400 cm⁻¹. The strong absorption band appearing between 1257 and 1144 cm⁻¹ is assigned to the CF₃ stretching mode. The absence of absorption within 3600–3200 cm⁻¹ confirms that the complexes are free from coordinated or absorbed water molecules. This statement is supported by the TGA data, since no significant weight losses were detected up to 105 °C.

3.3. Powder X-ray diffraction characterization

The PXRD analysis shows that complexes A, B, C, and D are all pure and single phase. Refined cell parameters are summarized in Table 1; experimental, simulated (using the Pawley method), and difference powder patterns are presented in Fig. 10 in the Supplementary materials. The diffraction peaks for complex D are broadened and the peaks with $d < 1.75$ are unobservable; the microcrystalline structure of complex D is less ordered than that of complexes A, B, and C.

3.4. Absorption and photoluminescence spectra

Optical absorption spectra of the neat *bath* ligand and the complexes with the *bath* ancillary ligand and A–D main ligands are presented in Fig. 2. The absorption spectra of the complexes exhibit two pronounced bands peaked at 280 and 320 nm that are characteristic of A–D ligands. It can be seen from the absorption spectra that increasing the degree of fluorination leads to the growth of the extinction coefficient. However, for complexes A and C relatively low extinction is observed due to their

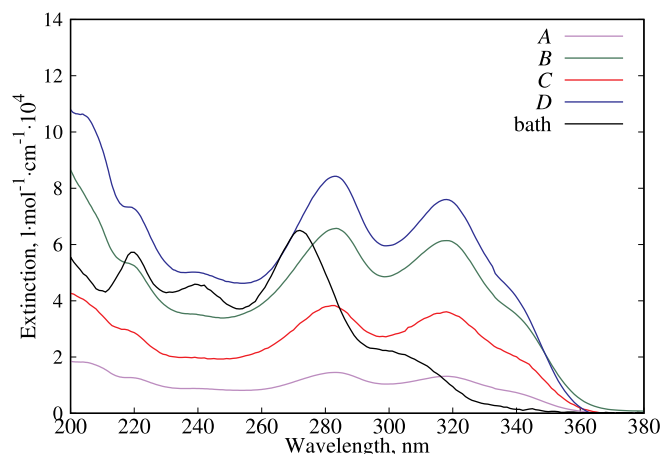


Fig. 2. Optical absorption spectra for investigated complexes and neat *bath* ligand dissolved in acetonitrile. Optical absorption of pure acetonitrile is presented by dashed curve.

symmetry. Two weak absorption maxima at 220 and 240 nm are associated with the absorption of the *bath* ligand.

Photoluminescence spectra of the neat ligands and complexes in solid phase are shown in Fig. 3. The PL spectrum of the neat *bath* ligand (curve 1 in panels A–D) has a complex structure with a maximum at 410 nm and a shoulder ranging up to 600 nm. Broad emission (400–700 nm) of the neat ligands A, B, and D has a single maximum located at 425, 410, and 525 nm, respectively, while the PL of ligand C exhibits multiple peaks within 470–480 nm (curve 2 in panels A–D). For all ligands the broad PL peaksssss are extended with a shoulder in the red spectral region. Successive increase in the degree of fluorination in ligands A–D leads to progressive shift of their emission to the long-wavelength region. Bonding *bath* and one of A–D ligands to Eu³⁺ results in an ion-centered luminescence of the complexes with complete suppression of the ligand emission (curve 3 in panels A–D). The observed narrow emission bands with maxima at 583 nm, 588 nm, 615 nm, 655 nm, and 680 nm are assigned to the ⁵D₀ → ⁷F₀, ⁵D₀ → ⁷F₁, ⁵D₀ → ⁷F₂, ⁵D₀ → ⁷F₃, and ⁵D₀ → ⁷F₄ transitions, respectively.

3.5. Optical excitation and absorption

Excitation spectra obtained for acetonitrile solutions of complexes A and C qualitatively resemble the corresponding optical absorption spectra (see curves 1 and 2 in panels A and C of Fig. 4). This means that complexes with spatial group $P2_1$ may have similar optical absorption and excitation spectra. Consequently, the quantum yield of these complexes does not depend on the excitation wavelength. For complexes B and D the maxima of the excitation spectra are shifted towards longer wavelengths by 40 nm with respect to the absorption edge. These maxima coincide with those observed in the excitation spectra for the solid samples. The differences between the excitation spectra recorded for the complexes in solid phase and the corresponding solutions arise from the concentration effects specific to solid samples.

3.6. Photoluminescence decays

Photoluminescence decays obtained for Eu³⁺ complexes (A–D) in solid phase are presented in Fig. 5. The measurements were carried out for the emission band corresponding to the ⁵D₀ → ⁷F₂ transition (615 ± 2 nm).

The experimental decays can be fitted with a single-exponential model

$$I_{th}(t) = Ae^{-t/\tau}, \quad (1)$$

where τ_i and A_i are the decay times and amplitudes, respectively. The measured luminescence decay is determined by

$$I_{exp}(t) = \int_0^{\infty} I_{irf}(t')I_{th}(t-t')dt'. \quad (2)$$

Here, the measured instrument response function $I_{irf}(t)$ (IRF) appears as a single exponent with the corresponding decay time of $\tau_{irf} = 1 \mu\text{s}$:

$$I_{irf}(t) = Ae^{-t/\tau_{irf}} \quad (3)$$

In order to eliminate the contribution from the instrument response function, the Levenberg-Marquardt deconvolution technique was employed. The resulting decays can also be presented as single-exponential curves. The corresponding characteristic times are presented in Table 2. From the obtained results we conclude that increasing the degree of fluorination in the ligand environment of the complexes does not greatly affect their PL decay times.

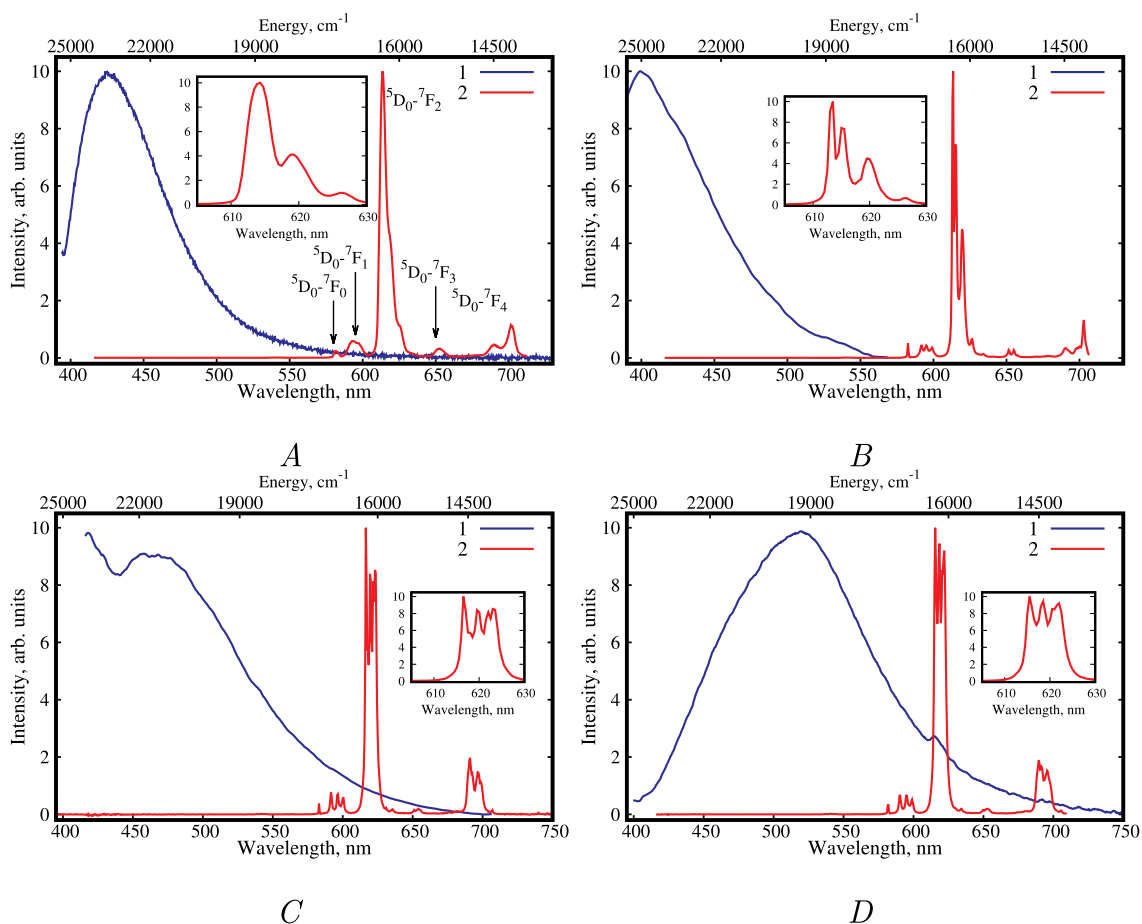


Fig. 3. Photoluminescence spectra of neat A–D ligands (1) and complexes (2) of Eu^{3+} ion, *bath*, and respective A–D ligands for solid samples excited by 365 nm CW radiation. Fine structures of PL spectra associated with ${}^5\text{D}_0 \rightarrow {}^7\text{F}_2$ transition in Eu^{3+} are shown in insets. Inset in panel A provides PL spectrum recorded at 77 K for complex A.

3.7. Quantum yields and sensitization efficiencies

The rate of the ${}^5\text{D}_0 \rightarrow {}^7\text{F}_1$ magnetic dipole transition in Eu^{3+} corresponding to the PL peak at 590 nm does not depend on the electric field induced by the ligand environment. Therefore, it is possible to evaluate the internal quantum yield from the normalized emission spectra by dividing the integrated intensities of the corresponding spectral bands by the integrated intensity of the magnetic transition [5,6,20]. The calculated internal quantum yields for complexes A–D are presented in Table 2.

The data on the measured radiative decay rates and external quantum yields are also provided in Table 2 together with the calculated internal quantum efficiencies, nonradiative decay rates, and sensitization efficiencies. The radiative decay rates A_{rad} for Eu^{3+} were calculated using the following relation [21,22]:

$$A_{\text{rad}} = A_{\text{MD}} n^3 \frac{I_{\text{TOT}}}{I_{\text{MD}}}, \quad (4)$$

where $A_{\text{MD}} = 14.65 \text{ s}^{-1}$ is the ${}^5\text{D}_0 \rightarrow {}^7\text{F}_1$ magnetic dipole transition rate for Eu^{3+} ion, $I_{\text{TOT}}/I_{\text{MD}}$ is the ratio of the total integrated emission to the integrated emission associated with the magnetic dipole transition. The refractive index n was taken to be 1.5. The nonradiative decay rate A_{nrad} was estimated using a simple relationship involving the calculated radiative decay rate A_{rad} and the observed decay time τ_{obs} :

$$A_{\text{nrad}} = A_{\text{rad}} - \tau_{\text{obs}}^{-1}. \quad (5)$$

From the data presented in Table 2 we conclude that increased degree of fluorination of the ligands in the complexes provides the growth of the photoluminescence quantum yields as the CF bonds have lower vibrational energy, thus, reducing the effect of quenching. Moreover, the extension of the fluorinated chain length results in a remarkable decrease in the rates of the nonradiative processes (see Table 2). However, saturation of the quantum yields observed for complexes C and D indicates that further increase in the degree of fluorination is unlikely to improve the quantum efficiency. This behaviour was recently reported for the complexes based on analogous Eu (III) 1,3-diketonates [5]. Replacing the ancillary ligand mentioned in Refs. [5,23] with *bath* increases the external quantum yield from 10.6% to 56% for complex C and from 11.4% to 55% for complex C, respectively.

3.8. Electroluminescence

In order to investigate the potential of the studied Eu^{3+} complexes for OLED applications, we developed and examined ITO/PEDOT:PPSS/ α -NPD/Eu complex:CBP/TPBi/LiF/Al OLED structures for each of the synthesized compounds. The average thickness of the obtained composite Eu complex:CBP active layers did not exceed ~ 40 nm, whereas the root-mean-square roughness of their surface was of about 8 nm (see results of atomic force microscopy (AFM) in Fig. 11 of Supplementary materials).

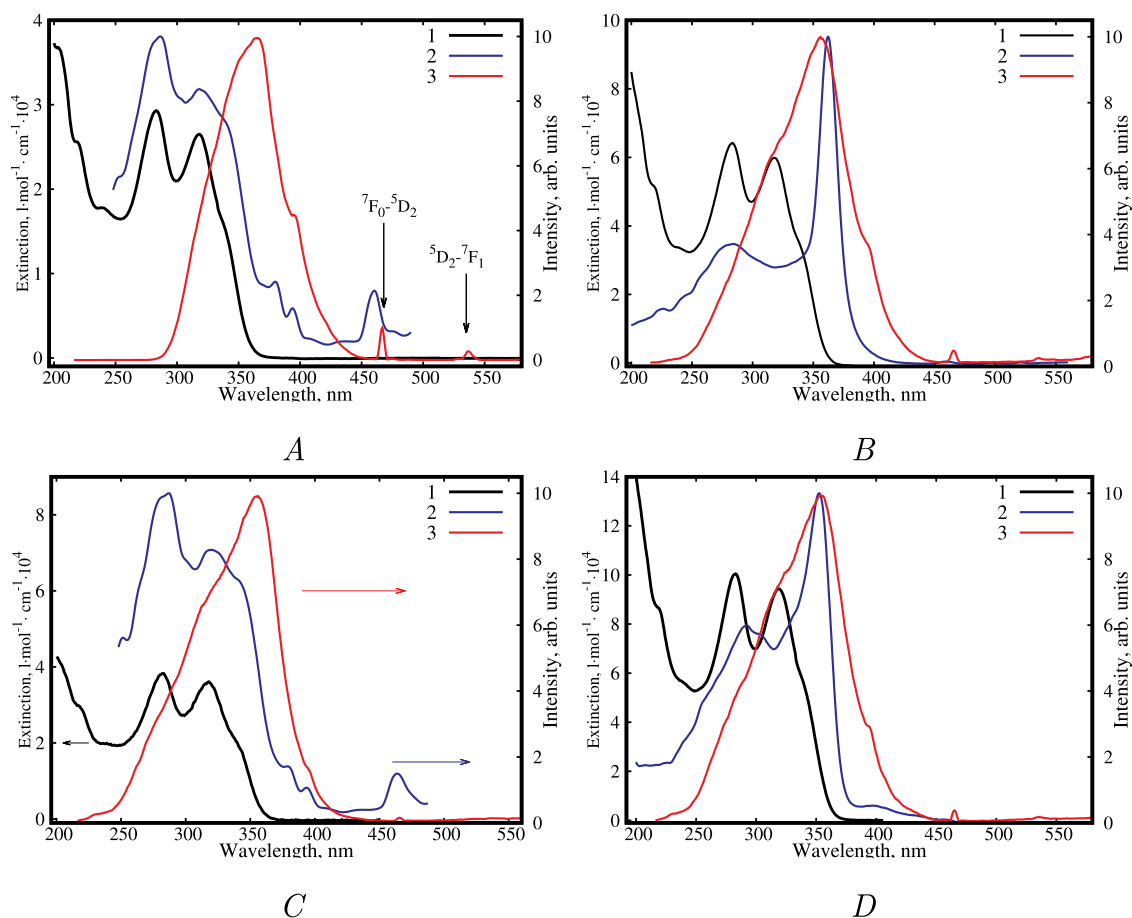


Fig. 4. Absorption spectra for complexes A–D dissolved in acetonitrile (1) and their excitation spectra for corresponding acetonitrile solutions (2) and solid samples (3) with emission recorded at 615 nm.

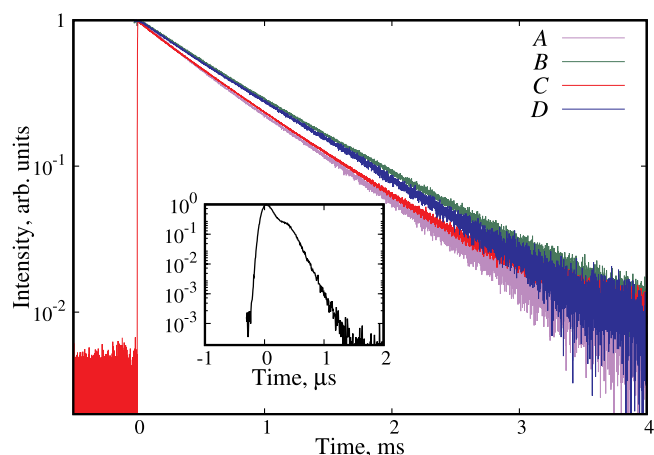


Fig. 5. Luminescence decays measured within 615 ± 2 nm emission band of investigated complexes under 355 nm pulsed laser excitation. Experiments were carried out for solid-state samples. Corresponding complexes are denoted with letters. Inset shows instrument response function (IRF).

The EL spectra of the devices exhibit pronounced peaks corresponding to the $^5D_0 \rightarrow ^7F_1$ transition in Eu^{3+} ion (see Fig. 6). The other transitions present in the photoluminescence spectra are also observed to a greater or lesser extent. The variation of the amplitudes of the low-intensity transitions in Eu^{3+} can be attributed to the influence of the

Table 2

Radiative (A_{rad}) and non-radiative (A_{nr}) decay rates, observed decay times (τ_{obs}) and their relative errors, internal and external quantum yields, and sensitization efficiencies.

	complex A	complex B	complex C	complex D
A_{rad}, s^{-1}	689	785	716	915
A_{nr}, s^{-1}	803	450	600	367
$\tau_{obs}, \mu s$	670	810	710	780
Relative error, %	1	1	1	2
Internal QY, %	46	64	57	71
External QY, %	27	39	56	55
Sensitization efficiency, %	59	60	99	77

electric field. A broad EL band ranging from 350 to 450 nm results from the electroluminescence of the CBP transport material (see Fig. 6, curve 4). A subtle peak detected at ≈ 540 nm probably corresponds to the $^5D_0 \rightarrow ^7F_1$ transition in Eu^{3+} ion. Notably, increasing the bias leads to the growth of the contribution from the CBP material. This effect most likely occurs due to the disbalance between the electron and hole currents, which entails the displacement of the recombination region in the OLED structure.

However, for the OLED based on complex A the EL band within 430–550 nm cannot be considered in the framework of the reasoning given above. We suggest that the regarded EL band is most likely associated with the appearance of exciplexes in the OLED structure [24]. To clarify the origin of this feature, we fabricated test films by thermal

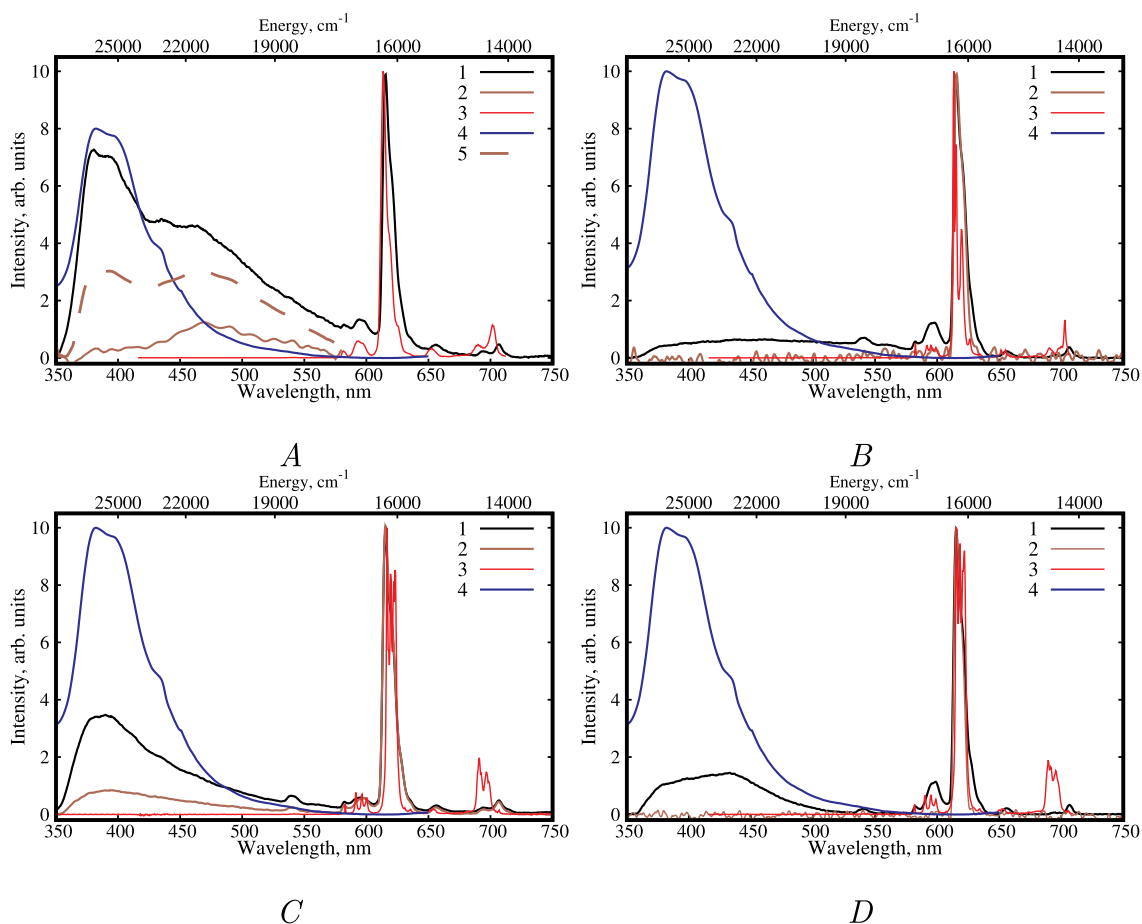


Fig. 6. Electroluminescence spectra at 12 V (1) and 8 V (2) obtained for ITO/PEDOT:PPS/ α -NPD/Eu complex:CBP/TPBi/LiF/Al organic light-emitting diodes; PL spectra for Eu^{3+} complexes A–D (3) and CBP transport material (4) measured under 365 nm excitation. In order to illustrate formation of exciplexes for OLED based on complex A, additional spectrum (5) measured at 10 V bias is provided.

coevaporation of complex A and CBP. In the PL experiments the spectrum of the film exactly matched the superimposed PL spectra of complex A and CBP with no emission bands observed within 430–550 nm. Thus, we conclude that the EL band at 430–550 nm can be attributed to formation of electroplexes [25,26].

The additional EL bands within 350–550 nm lead to a noticeable variation in the chromaticity of the devices (see Fig. 8). Therefore, it is potentially possible to fine-tune the device structure to achieve white emission with appropriate colour characteristics.

3.9. Electrophysical characteristics and photometric performance

All devices based on the studied complexes A–D exhibit characteristic non-linear behaviour of the J–V curves (see Fig. 7, panel 1) governed by two charge transport regimes ($J \propto V^n$, corresponding values of parameter n are given in Table 4 of Supplementary materials). In particular, the space-charge limited regime ($n \sim 2$) observed for the devices A and C at low applied voltages is followed by the trap-limited regime ($n > 2$) above ~ 6 V. Alternatively, at low voltages ohmic conduction is the most probable charge transport mechanism in the devices B and D since $n < 1$, whereas above ~ 8 V it is changed to the trap-limited regime. Visible electroluminescence appears at 4–6 V. These values of threshold voltages are comparable to the ones reported for analogous OLEDs based on metalorganic compounds [27], as well as for the hybrid OLEDs based on semiconductor nanoparticles [28,29]. The

luminance-voltage characteristics of the devices (see Fig. 7, panel 2) are similar except for the device B, which has the largest operating voltage of 10 V indicating the presence of a large potential barrier in the OLED structure. The highest obtained luminance was 70 cd/m^2 (device C). As expected, the OLED sample based on complex A reveals the poorest performance in terms of the current efficiency and external quantum efficiency due to rather high current densities within the device at low bias (see Fig. 7, panels 3 and 4). This fact indicates that the potential barrier in the active layer is small, which, in turn, gives rise to the charge carrier drift through the active layer, suppressing its electroluminescence. The highest achieved external quantum efficiency was $\sim 1\%$ (device C), which was slightly decreased at high voltages.

By comparing the results given in Tables 2 and 3 we conclude that the behaviour of the sensitization efficiencies qualitatively resembles that of the OLED quantum efficiencies depending on the degree of fluorination in the ligand environment of the complexes.

4. Conclusion

Thus, the influence of the degree of fluorination on the emissive properties of Eu^{3+} complexes with different β -diketonate main ligands and a 4,7-Diphenyl-1,10-phenanthroline (bathophenanthroline) ancillary ligand was investigated. The organic light-emitting diodes based on the investigated complexes were studied as well. It was demonstrated that the increase in the degree of fluorination of the main ligand in the

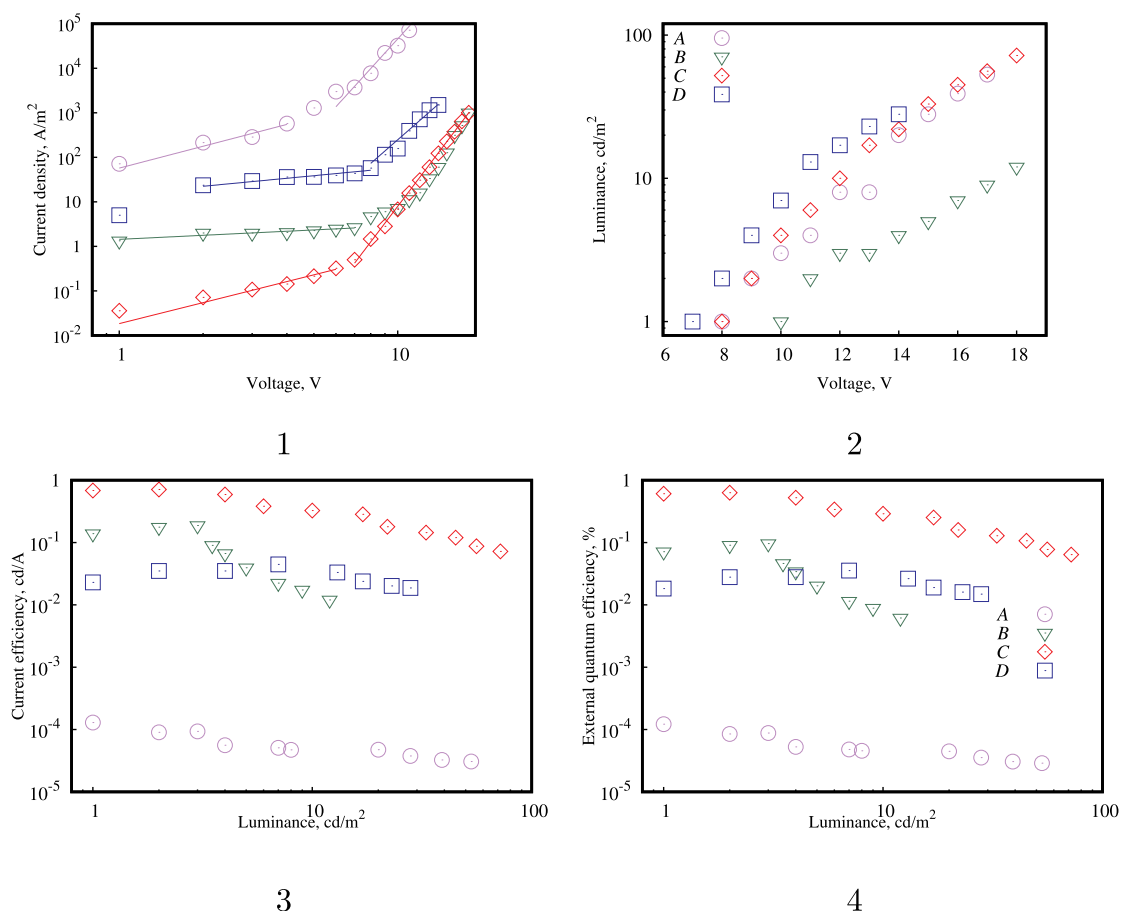


Fig. 7. Electrophysical and photometric performance for ITO/PEDOT:PPSS/ α -NPD/Eu complex:CBP/TPBi/LiF/Al OLED structures based on Eu^{3+} complexes: 1 – current density-voltage plot; 2 – luminance versus voltage; 3 – current efficiencies and 4 – external quantum efficiencies as functions of OLED luminance.

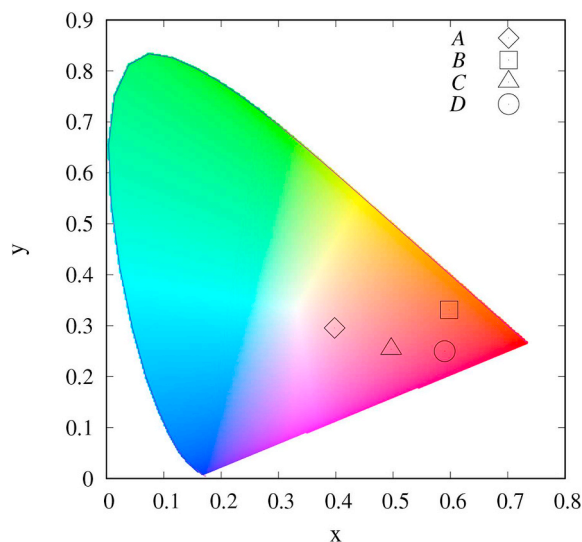


Fig. 8. CIE 1931 xy color space coordinates evaluated from EL spectra of ITO/PEDOT:PPSS/ α -NPD/Eu complex:CBP/TPBi/LiF/Al OLED structures based on investigated Eu^{3+} complexes A–D. (For interpretation of the references to colour in this figure legend, the reader is referred to the Web version of this article.)

Eu^{3+} complexes leads to the growth of their external quantum yields. For complexes C and D saturation of quantum yields was observed with maximum achieved QY values of 56%. Therefore, further fluorination of the ligands is unlikely to improve the emission efficiency of the complexes. It was shown that the evaluated quantum efficiencies of the

Table 3
Characteristics of OLEDs.

	OLED A	OLED B	OLED C	OLED D
Turn-on voltage, V	5.5	6	4.5	5
Max. luminance, cd/m^2	53 at 17 V	10 at 18 V	72 at 18 V	28 at 14 V
Max. quantum efficiency, %	4×10^{-4}	9×10^{-2}	7×10^{-1}	3×10^{-2}
Max. power efficiency, %	2×10^{-2}	3×10^{-2}	2×10^{-1}	1×10^{-2}
Operating voltage, V	8	10	8	10

OLEDs and the sensitization efficiencies reveal similar behaviour depending on the degree of fluorination of the ligands in the complexes. The maximum sensitization efficiency of 99% was achieved for complex C with the quantum efficiency of the corresponding OLED being 0.7%. These results can be employed in the design of the lanthanide complexes with highly efficient luminescence.

Acknowledgements

Synthetic and analytical parts of the work were supported by the Russian Science Foundation under project # 17-72-20088. Spectral measurements were funded by the Russian Foundation for Basic Research under projects # 16-02-00594 a, 18-02-00653 a, 16-29-11805 ofi_m. The X-ray diffraction data were obtained using the equipment at the Centre for molecules composition studies of INEOS RAS. A. A. Vashchenko, D. O. Goriachiy, and A. S. Selyukov also acknowledge the financial support from the Russian Foundation for Basic Research under project # 17-32-80050 mol_ev_a.

Appendix A. Supplementary data

Supplementary data to this article can be found online at <https://doi.org/10.1016/j.dyepig.2018.12.006>.

References

- [1] A. Vitukhnovsky, S. Ambrozevich, V. Korshunov, I. Taydakov, K. Lyssenko, M. Metlin, A. Selyukov, Luminescent properties of complexes based on scandium(III) β -diketonates, *J Lumin*:10.1016/j.jlumin.2018.03.053. URL <https://doi.org/10.1016/j.jlumin.2018.03.053>.
- [2] Strasser T. Phosphorescent platinum(II) complexes with $c\hat{c}^*$ cyclometalated NHC ligands. *Acc Chem Res* 2016;49(12):2680–9. <https://doi.org/10.1021/acs.accounts.6b00240><https://doi.org/10.1021/acs.accounts.6b00240>.
- [3] Metlina D, Metlin M, Ambrozevich S, Taydakov I, Lyssenko K, Vitukhnovsky A, Selyukov A, Krivobok V, Aminev D, Tobokhova A. Luminescence and electronic structure of nd^{3+} complex with pyrazole-substituted 1,3-diketone and 1,10-phenanthroline. *J Lumin* 2018;203:546–53. <https://doi.org/10.1016/j.jlumin.2018.07.005>.
- [4] Metlin M, Ambrozevich S, Metlina D, Vitukhnovsky A, Taydakov I. Luminescence of pyrazolic 1, 3-diketone pr^{3+} complex with 1, 10-phenanthroline. *J Lumin* 2017;188:365–70. <https://doi.org/10.1016/j.jlumin.2017.04.058><https://doi.org/10.1016/j.jlumin.2017.04.058>.
- [5] Varaskina E, Taydakov I, Ambrozevich S, Selyukov A, Lyssenko K, Jesus L, Freire R. Influence of fluorinated chain length on luminescent properties of eu^{3+} beta-diketonate complexes. *J Lumin* 2018;196:161–8. <https://doi.org/10.1016/j.jlumin.2017.12.006><https://doi.org/10.1016/j.jlumin.2017.12.006>.
- [6] Bünzli J-CG, Piguet C. Taking advantage of luminescent lanthanide ions. *Chem Soc Rev* 2005;34(12):1048. <https://doi.org/10.1039/b406082m><https://doi.org/10.1039/b406082m>.
- [7] Ebata T, Iwasaki A, Mikami N. Vibrational relaxation of oh and od stretching vibrations of phenol and its clusters studied by iruv pump-probe spectroscopy. *J Phys Chem* 2000;104(34):7974–9. <https://doi.org/10.1021/jp0015022><https://doi.org/10.1021/jp0015022>.
- [8] Taidakov IV, Zaitsev BE, Lobanov AN, Vitukhnovskii AG, Datskevich NP, Selyukov AS. Synthesis and luminescent properties of neutral eu(iii) and gd(iii) complexes with 1-(1,5-dimethyl-1h-pyrazol-4-yl)-4,4,4-trifluoro-1,3-butanedione and 4,4,5,5,6,6,6-heptafluoro-1-(1-methyl-1h-pyrazol-4-yl)-1,3-hexanedione. *Russ J Inorg Chem* 2013;58(4):411–5. <https://doi.org/10.1134/S0036023613040190><https://doi.org/10.1134/S0036023613040190>.
- [9] Bochkov MA, Vitukhnovsky AG, Taidakov IV, Vashchenko AA, Katsaba AV, Ambrozevich SA, Brunkov PN. Optimization of Carrier mobility in luminescence layers based on europium β -diketonates in hybrid light-emitting structures. *Semiconductors* 2014;48(3):369–72. <https://doi.org/10.1134/s1063782614030051><https://doi.org/10.1134/s1063782614030051>.
- [10] Freund C, Porzio W, Giovanella U, Vignali F, Pasini M, Destri S, Mech A, Pietro SD, Bari LD, Mineo P. Thiophene based europium β -diketonate complexes: effect of the ligand structure on the emission 315 quantum yield. *Inorg Chem* 2011;50(12):5417–29. <https://doi.org/10.1021/ic1021164><https://doi.org/10.1021/ic1021164>.
- [11] Yu J, Zhou L, Zhang H, Zheng Y, Li H, Deng R, Peng Z, Li Z. Efficient electro-luminescence from new lanthanide (eu^{3+}/tb^{3+} , sm^{3+}/tb^{3+}) complexes. *Inorg Chem* 2005;44(5):1611–8. <https://doi.org/10.1021/ic0485561><https://doi.org/10.1021/ic0485561>.
- [12] Lima P, Paz F, Brites C, Quirino W, Legnani C, e Silva MC, Ferreira R, Júnior S, Malta O, Cremona M, Carlos L. White OLED based on a temperature sensitive eu^{3+}/tb^{3+} β -diketonate complex. *Org Electron* 2014;15(3):798–808. <https://doi.org/10.1016/j.orgel.2014.01.009><https://doi.org/10.1016/j.orgel.2014.01.009>.
- [13] Xu H, Sun Q, An Z, Wei Y, Liu X. Electroluminescence from europium(III) complexes. *Coord Chem Rev* 2015;293–294:228–49. <https://doi.org/10.1016/j.ccr.2015.02.018><https://doi.org/10.1016/j.ccr.2015.02.018>.
- [14] Kalyakina AS, Utochnikova VV, Sokolova EY, Vashchenko AA, Lepnev LS, Deun RV, Trigub AL, Zubavichus YV, Hoffmann M, Mühl S, Kuzmina NP. OLED thin film fabrication from poorly soluble terbium o -phenoxybenzoate through soluble mixed-ligand complexes. *Org Electron* 2016;28:319–29. <https://doi.org/10.1016/j.orgel.2015.11.006><https://doi.org/10.1016/j.orgel.2015.11.006>.
- [15] Utochnikova VV, Solodukhin NN, Aslandukov AN, Marciniak L, Bushmarinov IS, Vashchenko AA, Kuzmina NP. Lanthanide tetrafluorobenzoates as emitters for OLEDs: new approach for host selection. *Org Electron* 2017;44:85–93. <https://doi.org/10.1016/j.orgel.2017.01.026><https://doi.org/10.1016/j.orgel.2017.01.026>.
- [16] Taydakov I, Krasnoselskiy S. An efficient synthesis of isomeric 1-(1-alkyl-1h-pyrazolyl) ethanones. *J Heterocycl Chem* 2012;49(6):1422–4. <https://doi.org/10.1002/jhet.869><https://doi.org/10.1002/jhet.869>.
- [17] Coelho AA. Indexing of powder diffraction patterns by iterative use of singular value decomposition. *J Appl Crystallogr* 2003;36(1):86–95. <https://doi.org/10.1107/s0021889802019878><https://doi.org/10.1107/s0021889802019878>.
- [18] B. A. TOPAS, V5.0, general profile and structure analysis software for powder diffraction data-user manual, Karlsruhe, Germany.
- [19] Pettinari C, Marchetti F, Pettinari R, Belousov YA, Taydakov IV, Krasnobrov VD, Petukhov DI, Drozdov AA. Synthesis of novel lanthanide acylpyrazolonato ligands with long aliphatic chains and immobilization of the tb complex on the surface of silica pre-modified via hydrophobic interactions. *Dalton Trans* 2015;44(33):14887–95. <https://doi.org/10.1039/c5dt01964h><https://doi.org/10.1039/c5dt01964h>.
- [20] Taidakov IV, Zaitsev BE, Lobanov AN, Vitukhnovskii AG, Datskevich NP, Selyukov AS. Synthesis and luminescent properties of neutral eu(III) and gd(III) complexes with 1-(1,5-dimethyl-1h-pyrazol-4-yl)-4,4,4-trifluoro-1,3-butanedione and 4,4,5,5,6,6,6-heptafluoro-1-(1-methyl-1h-pyrazol-4-yl)-1,3-hexanedione. *Russ J Inorg Chem* 2013;58(4):411–5. <https://doi.org/10.1134/s0036023613040190><https://doi.org/10.1134/s0036023613040190>.
- [21] Yu Y, Chen D, Huang P, Lin H, Wang Y. Structure and luminescence of eu^{3+} doped glass ceramics embedding ZnO quantum dots. *Ceram Int* 2010;36(3):1091–4. <https://doi.org/10.1016/j.ceramint.2009.12.007><https://doi.org/10.1016/j.ceramint.2009.12.007>.
- [22] Rakov N, Maciel GS. Upconversion luminescence enhancement of $Er^{3+}:Yb^{3+}$ doped Al_2O_3 powder containing Lu^{3+} . *Sci Adv Mater* 2013;5(4):380–4. <https://doi.org/10.1166/sam.2013.1468><https://doi.org/10.1166/sam.2013.1468>.
- [23] Taydakov IV, Akkuzina AA, Avetisov RI, Khomyakov AV, Saifutayrov RR, Avetisov IC. Effective electroluminescent materials for OLED applications based on lanthanide 1,3-diketonates bearing pyrazole moiety. *J Lumin* 2016;177:31–9. <https://doi.org/10.1016/j.jlumin.2016.04.017><https://doi.org/10.1016/j.jlumin.2016.04.017>.
- [24] Aroca R, Caño TD, de Saja JA. Exciplex formation and energy transfer in mixed films of phthalocyanine and perylene tetracarboxylic diimide derivatives. *Chem Mater* 2003;15(1):38–45. <https://doi.org/10.1021/cm020756s><https://doi.org/10.1021/cm020756s>.
- [25] Zhang Y, Hao Y, Meng W, Xu H, Wang H, Xu B. The characterization of electroplex generated from the interface between 2-(4-trifluoromethyl-2-hydroxyphenyl)benzothiazole] zinc and n, n'-diphenyl-n, n'-bis(1-naphthyl)-(1, 1'-biphenyl)-4, 4'-diamine. *Appl Phys A* 2011;106(3):709–15. <https://doi.org/10.1007/s00339-011-6677-5><https://doi.org/10.1007/s00339-011-6677-5>.
- [26] Yang S, Zhang X, Hou Y, Deng Z, Xu X. Charge carriers at organic heterojunction interface: exciplex emission or electroplex emission? *J Appl Phys* 2007;101(9):096101<https://doi.org/10.1063/1.2713947><https://doi.org/10.1063/1.2713947>.
- [27] Martins JP, Martín-Ramos P, Coya C, Silva MR, Eusebio MES, de Andrés A, Álvarez ÁL, Martín-Gil J. Highly luminescent pure-red-emitting fluorinated β -diketonate europium(III) complex for full solution-processed OLEDs. *J Lumin* 2015;159:17–25. <https://doi.org/10.1016/j.jlumin.2014.10.020><https://doi.org/10.1016/j.jlumin.2014.10.020>.
- [28] Vitukhnovskii AG, Vashchenko AA, Lebedev VS, Vasiliev RB, Brunkov PN, Bychkovskii DN. Mechanism of electronic-excitation transfer in organic light-emitting devices based on semiconductor quantum dots. *Semiconductors* 2013;47(7):971–7. <https://doi.org/10.1134/s1063782613070245><https://doi.org/10.1134/s1063782613070245>.
- [29] Vashchenko AA, Lebedev VS, Vitukhnovskii AG, Vasiliev RB, Samatov IG. Electroluminescence of CdSe/CdS quantum dots and the transfer of the exciton excitation energy in an organic light-emitting diode. *JETP Lett (Engl Transl)* 2012;96(2):113–7. <https://doi.org/10.1134/s0021364012140135><https://doi.org/10.1134/s0021364012140135>.